International Journal of Heat and Technology
Vol. 42, No. 4, August, 2024, pp. 1257-1269
Journal homepage: http://iieta.org/journals/ijht

Effect of LbL Deposited Chitosan-Nanosilica Bilayers on Flammability and Thermal Properties of Polylactide Materials

Tomasz M. Majka

Department of Chemistry and Technology of Polymers, Cracow University of Technology, Cracow 31155, Poland

Corresponding Author Email: tomasz.majka@pk.edu.pl

https://doi.org/10.18280/ijht.420416

Received: 19 June 2024
Revised: 18 August 2024
Accepted: 25 August 2024
Available online: 31 August 2024

Keywords:
biocomposites, flame retardants, flammability, Layer by Layer technique, nanosilica, polylactide

ABSTRACT

The present work is devoted to studying the effect of the synergistic action of Si-O-Si and NH-CO groups on the flammability and thermal properties of polylactide (PLA). For this purpose, using the Layer-by-Layer (LbL) technique, 5, 10, and 15 bilayers of chitosan (CS) and nanosilica (NS) were deposited onto the surface of PLA and PLA/NS composite (PLA/A200). More than a 20% reduction in flammability was achieved (sample (15BL) PLA/A200). Studying the effect of LbL-deposited bilayers on two types of surfaces, an identical relationship was found: the more layers adsorbed, the lower thermal stability, and vice versa the more layers, the higher flame retardancy. In turn, the lower the thermal stability, the faster the ability to form char, and the more solid residue, the lower the flammability and longer the burning time. This means that the application of CS-NS bilayers results in decomposition reactions in the condensed phase, which reduces the amount of flammable gases released.

1. INTRODUCTION

The literature offers some examples of the use of organic-inorganic hybrids as potential flame retardants (FR) for biomaterials such as polylactide [1-9]. Leading the way are systems of renewable compounds in combination with phosphorus compounds [10-12].

However, phosphorus-containing systems have some limitations. They are often solutions of phosphate salts, making them difficult to introduce into the desired system, especially at elevated temperatures. Secondly, phosphorus compounds are expensive and the use of too small amounts (2-3 wt.%) does not significantly change the flammability characteristics of the tested materials [13, 14]. Finally, to achieve a high class of fire resistance, it is necessary to use them in combination with nitrogen compounds [15-18]. Therefore, new, low-cost and effective solutions dedicated to polymeric biomaterials, especially biopolyesters, are currently being sought.

Such a compound is chitosan (CS, a polyaminosaccharide) produced mainly by partial deacetylation of chitin, which is widely distributed in nature, mainly as a structural component of crustacean exoskeletons. Chitosan is easily susceptible to organic modification due to its ability to bind with fats, proteins, or just metal ions. Microcrystalline chitosan is characterized by high adhesion, antibacterial activity, high chemical reactivity, and good miscibility with polymers [19-21].

Many scientific reports have used the Layer by Layer (LbL) technique to apply chitosan [22-25]. This is a simple technique used for the growth of hybrid manufacures, mainly in the area of biomaterials. The LbL technique offers several advantages over other thin film deposition methods. First, it is an inexpensive deposition method. Unfortunately, it requires much more time to cover a given surface than other methods. There is a wide range of materials that can be deposited using LbL. In addition, the technique is suitable for coating products with complex geometries, especially those containing sharp edges [26, 27]. Although deposition takes place at room temperature and allows for a reduction in surface porosity, it consumes rather large amounts of solvents and does not allow for dimensional control of the applied particles [28].

In a paper of Ghavidel Mehr et al. [29], the addition of chitosan via LbL was shown to be superior to the dip-coating technique. In the work of Liu et al. [30], to improve fire resistance, the LbL technique was used to deposit chitosan on the surface of cotton fabrics coated with sodium phytate and 3-aminopropyltriethoxysilane deposition of sodium phytate, chitosan and hydrolyzed aminopropyltriethoxysilane led to a reduction in the rate of heat release, total heat release, total smoke release and smoke generation rate. Ma et al. [31] have shown that the phosphorylation and phosphoramidation reactions of chitosan with phenylphosphoryl dichloride and tetraethylenepentamine, respectively, yield excellent flame retardancy of PLA. Such synergism of action between phosphorus compounds and chitosan towards reducing the flammability of PLA was also confirmed by Vahabi et al. [32] and Jing et al. [33], but it required the use of antipyrrole above 10% by weight.

Another promising component of the organic-inorganic hybrid is nanosilica (NS). Nanosilica is characterized by the high adsorption capacity of biomacromolecules including proteins therefore ideally suited for the chitosan-nanosilica system [34-38]. The development of new hybrid materials

based on chitosan and nanosilica opens up the possibility of combining both the favorable properties of silicas and the attractive features of chitosan in a single material [39]. The aforementioned synergy also lies in the mutual interpenetration of phases because NS effectively fills the pore structure of the chitosan network by which the thermal properties of these structures are improved [40]. In addition, CS especially in acidic environments has positive charges in amine groups (single NH_2 bond), which favor a number of interactions with NS silanol groups [41, 42].

Nanosilica also has high barrier properties. The publication of Ortenzi et al. [43] showed that the presence of NS nanoparticles, contributes to a significant increase in crystallinity and a decrease in permeability to O_2 and CO_2. The O_2 and CO_2 permeability values were reduced to 80% and 50%, respectively, compared to pure PLA.

Based on all the literature reports mentioned above, the purpose and scope of the experimental work were specified. The purpose of this work was to study the effect of CS-NS hybrid bilayers deposited by the LbL technique onto the surface of PLA and PLA/NS composite, on the flammability and thermal properties of the biopolymer matrix.

2. RAW MATERIALS

A polylactide (PLA, CAS No. 26100-51-6, M_w = 116000 Da, PDI = 1.83 [44]) with the trade name Ingeo™ Biopolymer 3052D purchased from NatureWorks (Blair, USA) was used to prepare reference samples. The polylactide composites were filled with AEROSIL®200 hydrophilic flame nanosilica (NS, A200, CAS No. 112945-52-5, 7631-86-9) from Evonik Industries AG (Hamburg, Germany). High molecular weight chitosan (CS, CAS No. 9012-76-4, reagent grade) manufactured by Sigma Aldrich (Darmstadt, Germany) and sold as a powder was also used to make the solutions.

3. ANALYTICAL METHODS

A JEOL JSM-6010LA analytical scanning electron microscope (JEOL Ltd., Tokyo, Japan) was used to confirm the adsorption of bilayers onto the surface of biomaterials. Images were taken at an accelerating voltage of 10 kV and a working distance of 10 mm. Before examination, each sample was sputtered with a 4 nm thick layer of gold.

PLA, PLA/A200 samples, and (BL)PLA and (BL)PLA/A200 composites were characterized by the following analytical methods.

Thermogravimetric (TGA) measurement was carried out on a NETZSCH TG 209F1 Libra apparatus (Netzsch, Krakow, Poland). The test was carried out on 5 mg samples in an oxidizing atmosphere under the following conditions: temperature range from 30 to 600°C; heating rate - 10°C/min.

The obtained biocomposites were examined for thermal changes using differential scanning calorimetry (DSC) on a Mettler Toledo DSC823e instrument (Mettler Toledo, Warsaw, Poland). The test was carried out in an inert atmosphere on samples of about 5 mg, according to the following temperature programs:

- heating 30-200°C at a rate of 10°C/min,
- cooling 200-30°C at a rate of 10°C/min,
- heating 30-200°C at a rate of 10°C/min.

Microcombustion calorimetry (MCC) was carried out using a Fire Testing Technology (FTT, East Grinstead, UK) apparatus in accordance with ASTM D7309. Measurements were carried out on 5 mg samples in the temperature range of 100-750°C at a heating rate of 1°C/s.

The UL-94 flammability test was conducted in UL94 HB (horizontal burning) and UL94 VB (vertical burning) modes in accordance with IEC 60695-11-10:1999/Amd 1:2003. In both modes, the test was conducted for 5 samples.

The limiting oxygen index (LOI) was measured using the Fire Testing Technology Oxygen Index apparatus (FTTOI, East Grinstead, UK) in accordance with ISO 4589-2:2017.

4. SAMPLE PREPARATION

A processing line consisting of a Brabender DR20 feeder (RHL-Service, Poznań, Poland), a Haake Rheomex OS PTW 16/25 twin-screw extruder (RHL-Service, Poznań, Poland), a Zamak W1500 cooling bath (Zamak Mercator, Skawina, Poland) and a Zamak G-16/325 peletizer (Zamak Mercator, Skawina, Poland) was used in the high-temperature processing (Figure 1).

With this laboratory processing line, PLA and PLA/A200 samples containing 5 wt.% of filler were obtained. Standard samples for LOI and UL94 testing were obtained using a P-200 compression press (Zamak Mercator, Skawina, Poland). All processing conditions are shown in Table 1.

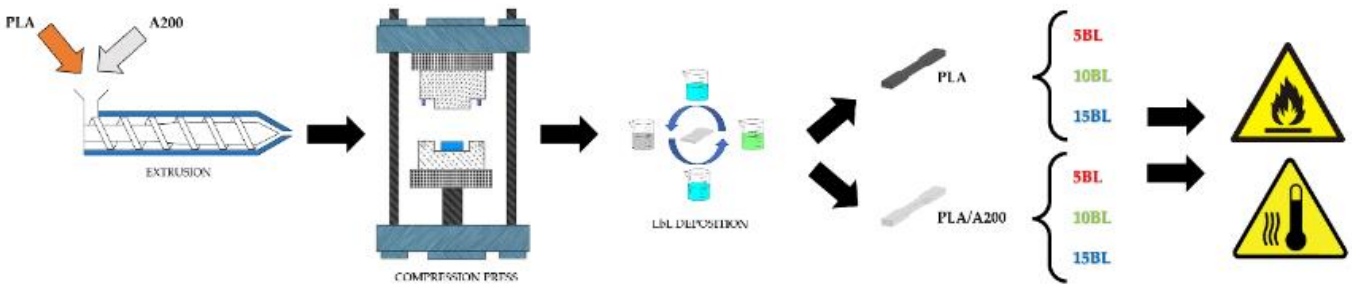

Figure 1. Schematic showing how biomaterials are obtained from high-temperature processing to bi-layer deposition using the LbL technique

Table 1. High temperature processing conditions

Extrusion							
Temperature [°C]	**Heating zones**						
	1	**2**	**3**	**4**	**5**	**6**	**Die**
	210	220	220	230	235	240	240
Degassing	-	-	-	-	Yes	-	-
Screws speed [rpm]	150						
Feed capacity [%]	5						
Cooling bath							
Temperature [°C]	25						
Compression press							
Temperature of stamps [°C]	235						
Pressure [Bar]	230						
Pressing time [s]	420						

5. SOLUTION PREPARATION AND LBL DEPOSITION

To obtain a 0.5% (m/m) solution of chitosan (CS) and nanosilica (NS), the raw materials were dissolved in 18.2 MΩ deionized (DI, CAS No. 7732-18-5) water (Hypernet, Poland). All mixtures were stirred with a magnetic stirrer for 8 h, and then their respective pH was determined. Using a 1 M hydrochloric acid (CAS No. 7647-01-0) solution (Chempur, Poland), the pH of the chitosan solution was set to 4.0±0.5, while with a 1 M sodium hydroxide (CAS No. 1310-73-2) solution (POCH, Poland) the pH of the nanosilica solution was stabilized to 9.8±0.1. The literature reports that CS completely adsorbs at acidic pH and NS at basic pH [45-49].

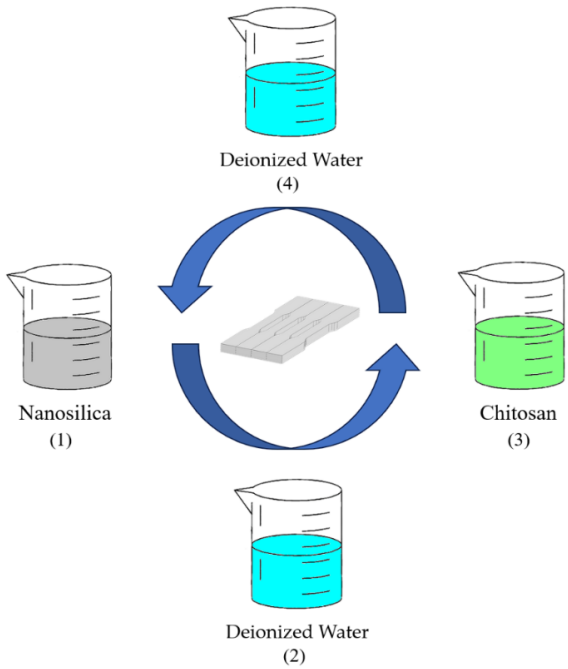

Figure 2. Diagram of the steps performed when applying bilayers using the LbL technique

Before deposition of the layers by the LbL technique, the surfaces of the materials were washed with DI. The samples were vacuum dried at 80°C for 2 hours. All samples were alternately immersed in a solution of nanosilica (NS) and chitosan (CS) to increase adhesion the first immersion in NS (1), CS (3) (Figure 2) was set for 5 minutes, but the subsequent immersion lasted only 1 minute. After each adsorption step, the materials were washed with DI for 1 minute to desorb poorly adsorbed compounds and dried for 30 minutes at 80°C. A schematic of the described procedure is shown in Figure 2. Each cycle was repeated until 5, 10, and 15 bilayers (BL) were built on each type of sample (e.g., (5BL) PLA means PLA with 5 bilayers deposited on the sample surface, and (10BL) PLA/A200 means PLA/A200 nanocomposite with 10 bilayers deposited by the LbL technique).

Figure 3 shows an SEM microphotograph of the surface of a representative sample of (10BL)PLA/A200 at 500x magnification. The surface was characterized by a solid structure, and streaks and undulations with smooth edges were noted on it, probably formed during processing. No obvious defects of the applied material layers were observed in the image.

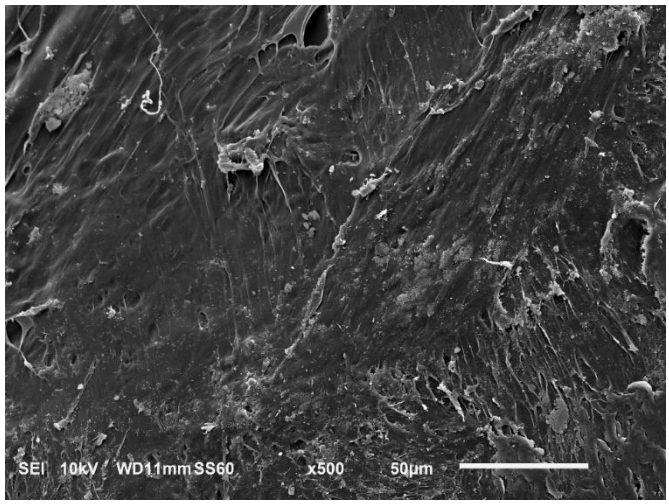

Figure 3. Microphotography of the surface of a (10BL)PLA/A200 sample at 500x magnification

In addition, mapping of the surface of the depicted structure was also performed to show the elements present on the surface of the material. Figure 4 presents the result of the aforementioned elemental analysis. The dependence of the number of counts on the radiation energy made it possible to indicate the elements present on the surface of the material under study. During the analysis, carbon was detected at an energy of 0.27 keV; nitrogen, 0.40 keV; oxygen, 0.52 keV; silicon, 1.74 keV; and gold at energies of 1.67 keV, 2.13 keV, and 2.43 keV. The occurrence of signals from N and Si suggest that chitosan and nanosilica are present on the surface, respectively.

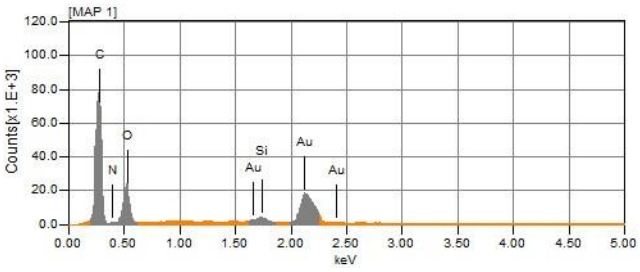

Figure 4. Elemental analysis for (10BL)PLA/A200 sample

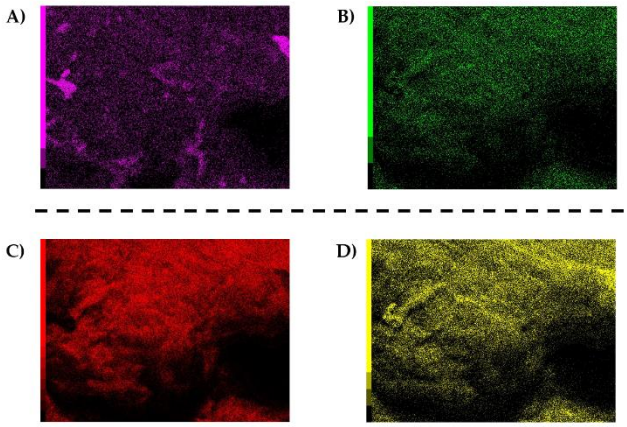

Figure 5. Elemental distribution on the surface of the (10Bl)PLA/A200 sample obtained with an X-ray energy detector (EDX): A) Silicon; B) Nitrogen; C) Carbon; D) Oxygen

The presented maps of the distribution of elements on the surface of the composite sample obtained with the X-ray energy detector (EDX) are the collective result of the intensity of the radiation pulses and the pixel size of the maps over the selected measurement area (Figure 5). The surface of the material was uniformly covered with the elements detected during the analysis. This shows that layers of nanosilica and chitosan were applied regularly. The small agglomerations seen in the Si image may be indicative of the non-uniform dispersion of nanosilica during the extrusion of the composite material or the formation of clusters of nanosilica during the application of layers by the LbL method. In addition, the distribution of Si and N elements in relation to C and O is different which may indicate the different degree of dispersion of nanosilica at submicron and nanometer levels, present both in the matrix and on the surface of the sample.

6. RESULTS AND DISCUSSION

6.1 Thermogravimetry analysis (TGA)

The results of the thermogravimetric analysis illustrate the two-stage degradation of the biomaterials (Figure 6). The course of all thermograms is very similar to each other except for the reference sample. It can be assumed that the effect of CS and NS is small on the thermal properties of the biomatrix. However, there are two areas where differences in the mass-temperature relationship are noticeable. The first is the area measured up to the $T_{5\%}$ point, where the thermal stability of PLA is about 10°C lower than samples containing bilayers (Table 2).

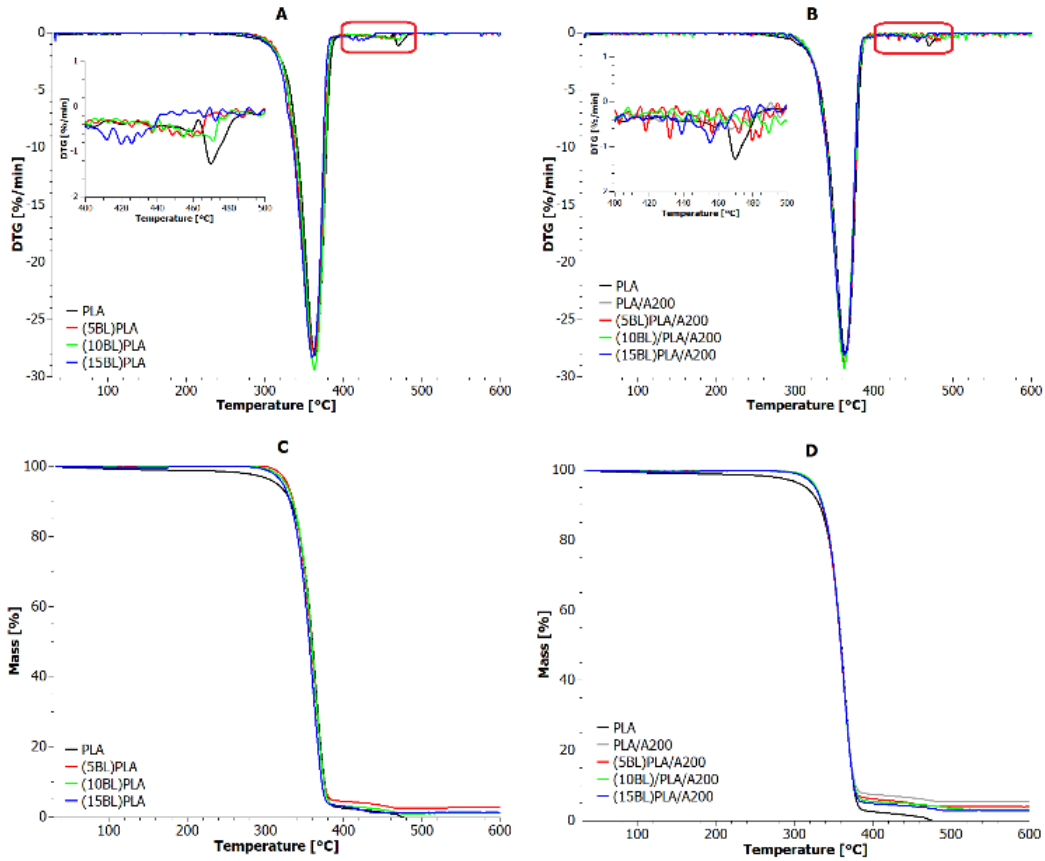

Figure 6. DTG (A-B) and TGA (C-D) curves for PLA and PLA/A200 samples deposited with 5, 10 and 15 CS and NS bilayers

Table 2. TGA indices determined for PLA and PLA/A200 samples based on Figure 6

Sample	$T_{5\%}$ [°C]	$T_{10\%}$ [°C]	$T_{20\%}$ [°C]	$T_{50\%}$ [°C]	T_{MAX} [°C]	Residue at 600°C [%]
PLA	315	332	344	360	364	0.00
(5BL)PLA	323	332	341	356	360	1.10
(10BL)PLA	326	335	345	359	363	1.27
(15BL)PLA	328	336	344	358	363	2.75
PLA/A200	328	336	345	360	362	5.39
(5BL)PLA/A200	327	336	345	359	363	3.96
(10BL)PLA/A200	328	336	345	360	362	3.20
(15BL)PLA/A200	326	335	345	359	363	2.80

In the area of highest mass loss, the thermograms almost overlapped up to the T_{ENDSET} point. On the other hand, the second is the area of charring afterburning noted from the T_{ENDSET} point to ~500°C. It is in this area that the real impact of bilayers on the PLA combustion mechanism can be seen. The differences are mainly due to the type of substrate used and the number of deposited layers. Figures 6A and 6C show graphs for PLA samples deposited with bilayers. The peak of the second stage of decomposition for PLA was at 470°C, and it shifted toward lower temperatures as the number of applied layers increased. Homogenization of NS in the PLA melt resulted in only a few degrees of shift in the peak point of the mass loss rate (Figure 6B and 6D). In contrast, the increase in the deposited layers tended to shift this peak toward higher temperatures, reaching as high as 490°C. In other words, adsorption of CS and NS bilayers onto the PLA surface leads to acceleration of the material's charring process, while adsorption of the same layers onto the PLA/A200 composite surface promotes delayed char formation.

The form of the substrate as well as the amount of deposited bilayers also affects the amount of carbon residue after thermo-oxidative decomposition. Pure PLA burns completely with the release of volatiles, yielding no residue. In contrast, covering the surface of the biopolymer with 5 and 10 bilayers leads to a solid residue of about 1%. A threefold increase in the concentration of CS and NS on the PLA surface also results in a nearly threefold increase in the char generation. Since pure PLA decomposes completely into gaseous products, it can be surmised that close to 5% of the decomposition residue of the PLA/A200 composite comes from the 5% share of NS in PLA. Meanwhile, as the layers applied onto the PLA/A200 biocomposite surface increase, the amount of carbon residue at 600°C gradually decreases. The observed trend can be explained by the effect of entrainment of light NS nanoparticles, simultaneously by the stream of oxygen flowing in the measurement chamber and escaping volatiles. Note that NS has a specific surface area of 200 m^2/g, an average particle size of 12 nm, and a low bulk density of 50 g/l [50], making it a highly dusty material, especially under fluctuating mass and temperature conditions. Thus, the higher the concentration of CS-NS on the PLA/A200 surface, the higher the residue loss.

6.2 DSC vs TGA

The objective of Differential Scanning Calorimetry (DSC) was to study the effect of the number of adsorbed bilayers on the phase transformations of the polylactide observed with a constant rise in temperature. Importantly, DSC curves were contrasted with TGA thermograms over the same measurement range (Figure 7). This gives an idea of the scale of mass loss during the occurrence of all the phase transformations shown.

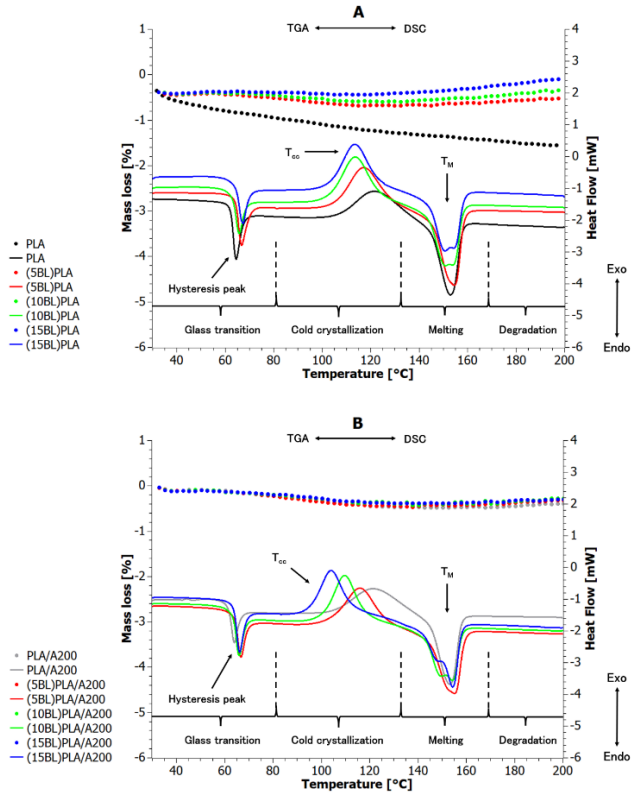

Figure 7. DSC curves for the samples: (A) PLA; (B) PLA/A200; deposited with 5, 10, and 15 bilayers along with the corresponding mass loss curves from 30-200°C

Heat flow curves for all analyzed biomaterials over the entire measurement range were characterized by the dominant phenomenon of energy absorption by the system. The biomaterials showed a negative energy effect throughout the entire cycle of the conducted test. As the number of bilayers applied onto the surface of PLA and PLA/A200 increased, the negative energy effect decreased relative to pure PLA. At 61-64°C, the midpoints of inflection of the curves were recorded, which were noted as the glass transition temperature of the material (Table 3). The addition of NS to the biopolyester matrix as well as the coating of the surface with CS and NS layers had virtually no effect on the shift of the transition point from the glassy state. However, the surface modification carried out had a weak but noticeable effect on the energy effect accompanying this transition. This means that covering the surface of PLA, ten or more bilayers makes it more difficult to melt the sample. In turn, to melt composite samples covered with bilayers, less energy must be supplied than is the case with the reference sample.

Table 3. DSC indicators where: melting temperature (T_m), melting enthalpy (ΔH_m), change in the heat capacity (ΔC_P), cold crystallization temperature (T_{cc}), and glass transition temperature (T_g)

Sample	T_g [°C]	ΔC_p [J/(g·K)]	T_{cc} [°C]	$T_{m\,1}$ [°C]	$T_{m\,2}$ [°C]	ΔH_m [J/g]
PLA	64	0.50	122	-	153	23.12
(5BL)PLA	64	0.50	117	-	156	28.43
(10BL)PLA	62	0.54	113	151	154	27.18
(15BL)PLA	63	0.56	113	151	154	26.80
PLA/A200	61	0.47	121	-	153	22.59
(5BL)PLA/A200	63	0.41	116	-	155	26.72
(10BL)PLA/A200	62	0.48	109	150	154	25.49
(15BL)PLA/A200	63	0.53	104	148	154	24.79

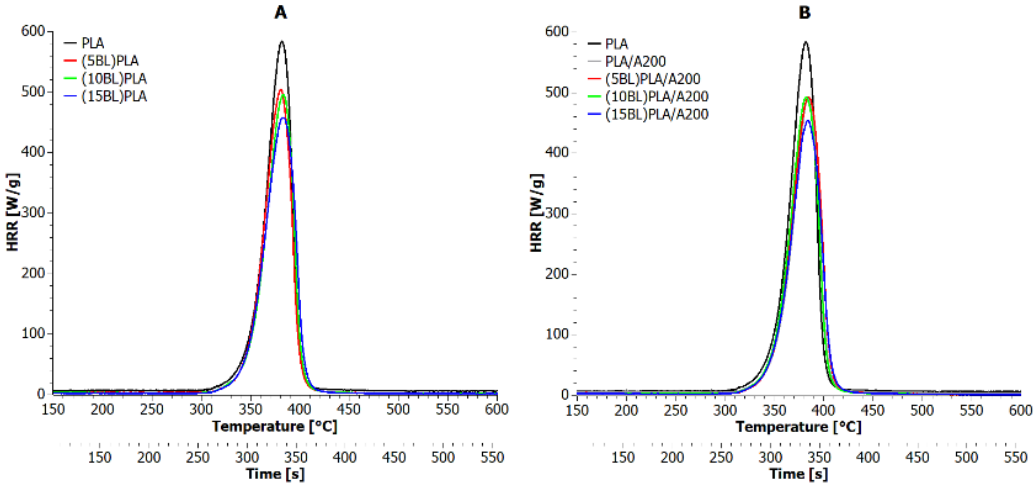

Figure 8. Heat release rate versus temperature and time for: A) PLA deposited by 5, 10 and 15 bilayers; B) PLA/A200 composites PLA deposited by 5, 10 and 15 bilayers

With a further increase in temperature, cold crystallization appeared. This phenomenon observed in polyester materials, among others, is associated with a rather delayed response of the material to changes in its environment. The fact is that with the number of applied bilayers, there is a shift in the peak of cold crystallization by up to several tens of degrees towards lower temperatures. This may be a rationale for supposing that the presence of CS microparticles and NS nanoparticles not only within the condensed phase but also on its surface, may contribute to the nucleation of crystalline phases within the near-surface layer rather than the core of the sample (accelerating the occurrence of the cold crystallization effect at lower temperatures).

A further phase transformation observed was the melting of the samples. PLA and PLA/A200 samples containing 10 and 15 bilayers on the surface were characterized by two characteristic melting peaks, the others by only one. PLA can crystallize in three crystalline forms [51-56]. The most common and stable polymorph is the α form, which is most often formed when PLA crystallizes from a melt. The β form can be obtained using high tensile and high-temperature conditions. The γ form can be obtained by epitaxial crystallization on a hexamethylbenzene substrate. Focusing on the crystallization of PLA from the melt as we have in this case, PLA can also crystallize into a disordered crystal called α'. This α' metaphase has an identical conformation to the α form, but looser packing and lower density [57, 58]. When crystallization occurs at below 115°C both α and α' phases are formed. At the same time, if cold crystallization occurs below 110°C the dominant phase is the α phase, while when crystallization occurs at temperatures of 110-115°C the dominant phase is the metastable α' phase [58, 59]. According to the thesis, deposition above 10 bilayers onto PLA promotes nucleation of the dominant α' metaphase, while adsorption above 10 bilayers on the PLA/A200 surface mainly results in nucleation of the stable α phase. The number of applied bilayers or the type of substrate used does not affect the melting temperatures of these phases.

It is also worth referring to the mass loss in the measurement range in question. Pure PLA, with a constant increase in temperature, loses mass linearly until it reaches 1.3% at 200°C, which may be related more to moisture loss and small initial degradation of the sample. Adsorption of bilayers on PLA initially promotes a small loss of mass, followed by a small increase in mass in the melting and degradation range. This swelling effect was observed only for PLA samples (the greater adsorption, the greater swelling). PLA/A200 composites practically in the range up to 200°C were stable in terms of mass (ΔM=0.3%), and the number of deposited layers did not affect its loss.

6.3 Micro Combustion Calorymetry (MCC)

Measurement of the Heat Release Rate (HRR) as a function of time and temperature (Figure 8) is characterized by several indicators (Table 4): PHRR - the peak of the HRR curve, TTI - Time To ignition, TOF - Time Out Flame.

The PHRR for PLA was 584 W/g. The addition of 5 wt.% NS to PLA resulted in a 16% loss of PHRR. Virtually the same effect can be obtained by applying 10 bilayers of CS and NS onto the PLA surface. The LbL technique used a 10 times lower weight of NS than during homogenization in the melt. Interestingly, adsorption of 5 and 10 bilayers on PLA/A200 did not affect the flammability of the composite sample at all.

The best PHRR reduction effect was obtained for all samples coated with 15 bilayers (22% flammability reduction).

Table 4. Summary of basic flammability indices for PLA/A200 samples

Sample	PHRR [W/g]	TTI [s]	TTI [°C]	TOF [s]	TOF [°C]	Combustion Time [s]
PLA	584	313	350	364	400	51
(5BL)PLA	505	297	344	355	401	58
(10BL)PLA	495	307	348	364	404	57
(15BL)PLA	458	305	346	368	407	63
PLA/A200	490	304	352	357	405	53
(5BL)PLA/A200	492	310	348	369	406	59
(10BL)PLA/A200	492	306	348	366	407	60
(15BL)PLA/A200	454	301	348	362	408	61

The presence of CS and NS also affected the flash point and quench point of the burned samples. All of the samples with bilayers ignited faster than PLA and generally extinguished later. Thus, the consequence of lowering PHRR relative to PLA was to increase the combustion time of biomaterials. No less the effect of the number of layers applied on the combustion time was small, as very similar results were obtained for both (5BL) and (15BL) samples. However, it is worth noting that much better results were obtained by the LbL technique deposition than by homogenization of the nanofiller in the biopolymer melt.

6.4 MCC vs TGA

Using ASTM D7309, additional flammability indices such as fire growth capacity (FGC) and heat release capacity (ηc), specific heat released (h_c also known as Total Heat Released - THR), pyrolysis residue, and specific heat of combustion gases were determined. The values of these indicators are summarized in Table 5.

The addition of NS to the polyester melt did not significantly change the start fire ability, but the application of 5, 10, and 15 bilayers onto the surface of PLA and PLA/A200 increased this ability twofold. This confirms the previously stated characteristic of the bilayers to ignite earlier than the core of the sample. At the same time, all samples showed a reduced heat release capacity compared to PLA. The higher the number of applied layers, the lower the η_c values. As a result, a nearly 25% reduction in η_c was recorded for the (15BL)PLA and (15BL)PLA/A200 samples. An identical relationship was observed during h_c analysis. With the application of 15 bilayers (regardless of the substrate) resulted in a 20% reduction in h_c relative to PLA.

Table 5. Flammability factors for polylactide biomaterials calculated according to ASTM D7309 standard

Sample	$T_{5\%}$ [s]	$T_{5\%}$ [K]	$T_{95\%}$ [s]	$T_{95\%}$ [K]	FGC [J/gK]	η_c [J/gK]	h_c [kJ/g]	$h_{c\ gas}$ [kJ/g]	Y_P [%]
PLA	243	552	495	811	179	650	22.90	22.90	0
(5BL)PLA	285	604	356	675	321	555	18.52	18.52	0
(10BL)PLA	290	603	362	675	317	540	18.46	14.79	20
(15BL)PLA	298	611	364	676	340	500	18.29	14.56	20
PLA/A200	230	549	388	712	192	539	18.99	3.18	83
(5BL)PLA/A200	296	607	367	677	341	541	19.48	19.48	0
(10BL)PLA/A200	294	609	363	677	336	540	18.73	18.73	0
(15BL)PLA/A200	292	612	360	679	328	492	18.13	15.94	12

As indicated by thermogravimetric studies, PLA decomposes completely into gaseous products, leaving no solid residue. The incorporation of NS nanoparticles into the biopolymer resulted in the highest recorded values of the solid residue after thermo-oxidative decomposition. Also, the results of the MCC analysis confirm the previous relationship. With that said, a 6-fold increase in the heating rate of the PLA/A200 composite generates a 16-fold higher solid residue after combustion. Covering the surface of PLA and PLA/A200 biocomposite with 5 bilayers of CS and NS is ineffective, as these samples also burn completely to gaseous products along with which light NS particles leave the system. Similar conclusions were made for the (10BL)PLA/A200 sample. The most effective solution turned out to be covering both surfaces with 15 bilayers of CS and NS. In both cases, there was a change in the combustion mechanism of the continuous phase and the generation of solid char. This may mean that the real impact on the formation of solid char has not only the synergistic action of Si-O-Si and NH-CO groups alone but *de facto* their respective amounts.

One of the most important characteristics of a material that controls its fire properties is the amount of gas phase and condensed phase released. Reducing the amount of gas phase released is one of the most effective approaches to blocking combustion. Increasing carbonization reduces the amount of gas and condensed phase released and increases the amount of residue. Chitosan is mainly responsible for the charring that occurs, which was also confirmed in a publication [60].

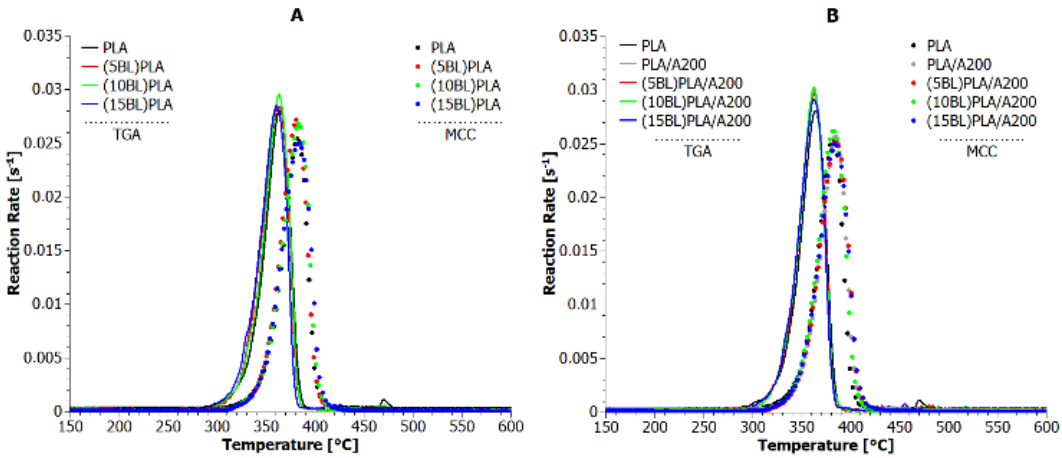

Figure 9. Reaction Rate calculated from TGA and MCC results for A) PLA deposited by 5, 10, and 15 bilayers; B) PLA/A200 composites PLA deposited by 5, 10, and 15 bilayers

Figure 9 shows the decomposition reaction rates (RR) determined for PLA and PLA/A200 composites based on MCC and TGA measurements. The differences between the observed peaks of the RR curves for the different measurement techniques are no more than 20°C. This means that regardless of the measurement method used, and the heating rate of the sample, all materials undergo complete decomposition in virtually the same temperature range. In contrast, the presents of filler and applied bilayers manifests a slight variation in these values.

Comparison of the results obtained from the two measurement methods (TGA and MCC), is also possible by determining the values of Overall Thermal Stabilization Effect (OSE) and Overall Flame Retardancy Effect (OFRE) in the same temperature range using the following Eqs. (1) and (2) [61-63]:

$$OSE = \sum_{T=150}^{600} \left((mass\ percent\ of\ polymer\ material_T) - (mass\ percent\ of\ polylactide_T)\right) \quad (1)$$

$$OFRE = \sum_{T=150}^{600} \left((HRR\ percent\ of\ polylactide_T) - (HRR\ percent\ of\ polymer\ material_T)\right) \quad (1)$$

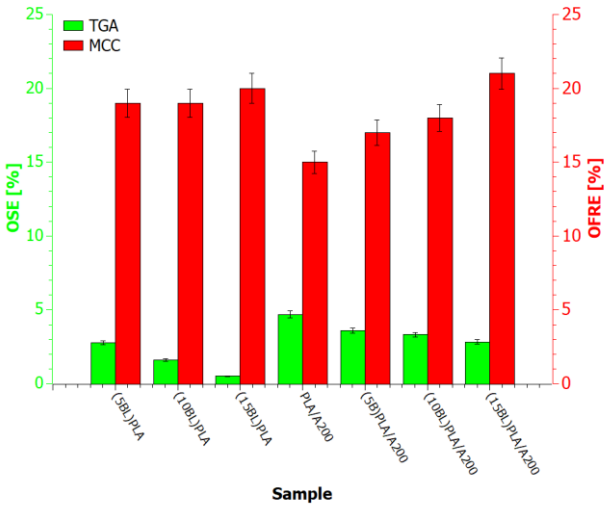

Figure 10. Overall Thermal Stabilization Effect (OSE) and Overall Flame Retardancy Effect (OFRE) for all tested PLA materials

The resulting OSE and OFRE ratios relating to the reference sample are summarized in Figure 10. Studying the effect of LbL-deposited bilayers on two types of surfaces, pure PLA and PLA/A200 nanocomposite, an identical relationship was found: the more layers adsorbed, the lower the OSE, and *vice versa* the more layers, the higher the OFRE. In contrast, the lower the thermal stability, the faster the ability to form char, and the more solid residue, the lower the flammability and longer the burning time.

6.5 UL-94 test

Table 6 shows the results of the UL-94 test in the vertical mode. When this measurement was carried out, there was a decrease in the viscosity of the biomaterial due to the rapid increase in temperature. As a consequence, hot melt sprang from all the tested samples without exception, which ignited the cotton placed under the samples. The base sample burned for less than a minute, and the addition of 5 wt.% nanofiller extended the average burning time of the composite by only 30 s relative to PLA. In general, as the number of applied layers increased, the combustion time of biomaterials increased. Applying 15 bilayers onto the PLA surface resulted in a doubling of the combustion time of the samples. Although among PLA/A200 composites the adsorption of 15 bilayers also proved to be the best, it did not achieve the same effect as on the PLA surface. The classification carried out quite transparently shows that in the case of composite samples containing applied bilayers, it was not possible to classify into any of the given standard categories. Based on this summary, it can be concluded that the adsorption of CS and NS in the form of layers did not reduce the flammability class of both polylactide and biocomposite materials.

The vertical orientation of the sample promotes rapid movement of the flame from the bottom to the top. Virtually all of the heated pure PLA flows with the flame onto the fabric beneath it. The sudden temperature change reduces the viscosity of the melt, which lacks the additional forces that maintain the geometry of the sample. The use of NS prolongs the cohesion effect but is still not sufficient to effectively counteract gravitational forces. The presence of bivariate layers on the PLA/A200 sample or 10BL and 15BL on the PLA, leads to visible effects in a relatively short time. As the number of falling droplets decreases, the burning time of the samples increases. This is because the NS particles in the CS combination form a physical insulator of the sample core against access to the flame. When the fabric is heated, both the biomatrix and low-molecular-weight organic compounds are rapidly decomposed into gaseous products. The gaseous products cause the mineral layer in between to clump together, creating temporary scaffolds that hold the sample geometry together for a much longer time.

Table 6. Measurement results using the UL-94 VB mode

Sample	Average Combustion Time [s]	Fabric Inflammation	Standard VB Classification
PLA	54±2	YES	FV-2
(5BL)PLA	53±2		FV-2
(10BL)PLA	73±2		FV-2
(15BL)PLA	119±2		FV-2
PLA/A200	83±2		FV-2
(5BL)PLA/A200	90±2		-
(10BL)PLA/A200	90±2		-
(15BL)PLA/A200	96±2		-

Table 7. Measurement results using the UL-94 HB mode

Sample	Average Combustion Time [s]	Average Combustion Rate [mm/min]	Average Length of the Burned Section [mm]	Average Number of Drops	Standard HB Classification
PLA	67±2	25.07±0.01	28±1	148±1	FH-2-28.00 mm/min
(5BL)PLA	126±2	31.22±0.01	51±1	371±1	FH-3-37.50 mm/min
(10BL)PLA	148±2	28.50±0.01	75±1	472±1	FH-3-31.69 mm/min
(15BL)PLA	159±2	23.34±0.01	75±1	556±1	FH-3-35.71 mm/min
PLA/A200	136±2	34.45±0.01	75±1	88±1	FH-3-39.47 mm/min
(5BL)PLA/A200	129±2	34.80±0.01	75±1	78±1	FH-3-35.16 mm/min
(10BL)PLA/A200	134±2	33.92±0.01	75±1	84±1	FH-3-38.14 mm/min
(15BL)PLA/A200	145±2	31.55±0.01	75±1	93±1	FH-3-35.71 mm/min

Table 7 shows the results of the UL-94 test in the horizontal mode. The reason for the incomplete combustion of PLA was the entrainment of the flame by detaching parts of the polymer melt. The pure polylactide sample was the only one that showed a tendency to flow during the conducted measurement. The visual evaluation made it possible to compare the tested materials in terms of combustion behavior in the very first seconds of the measurement and to draw the first conclusions. Looking at the results in Table 7 for PLA, one might be under the mistaken impression that the biopolymer has the best flammability rating because it self-extinguishes shortly after the flame is removed. Nothing could be further from the truth. Polylactide has very low viscosity at elevated temperatures. A biopolymer sample suspended at an appropriate height, containing a moving heat source at the end, was elastically deformed in the direction of gravity. The absence of any physical forces binding the polymer chains together, located within the burned material, and the increasing temperature were the reasons why parts of the test material detached rather quickly along with the flame. As a result, the flame was not extinguished but moved with the melt making the material very dangerous and susceptible to initiation of other ignition points as evidenced by the high value of the flame spread factor (PHHR/TTI). In general, the polylactide materials were characterized by a large number of small droplets of burned material falling off during the test. As in other measurements, the burning time of PLA samples generally increased as the number of applied bilayers increased, which may suggest that the presence of interlaced Si-O-Si and NH-CO groups impedes flame propagation. In contrast, the number of droplets decreased significantly for the composite samples, but they were much larger than for the polylactide materials. It can be assumed that it is mainly due to the presence of NS nanoparticles also in the composite structure. Flammability classification according to this method depended mainly on the length of material burned and the speed of combustion. Because the biopolymer matrix still does not lose its tendency to form bubbles during combustion, but the presence of the NS-CS system allows the movement of inorganic particles in the matrix in such a way that a temporary structure is formed on the surface of the sample, bonding the entire geometry by cutting off the core's access to oxygen. As a result, the fewest droplets are detached, which, if they fall, do not contain an open source of flame.

6.6 Limited Oxygen Index (LOI)

Measurement of the limiting oxygen index started with PLA, for which 19.3% was chosen as a reference point. Figure 11 shows the LOI values obtained for all biomaterials tested.

The literature reports showed, that PLA is a flammable biopolymer with an LOI of 19% [64]. NS is mainly responsible for the formation of the epidermal barrier layer. The use of a nanoadditive with high thermal conductivity can increase the rate of heat dissipation from a burning biocomposite [65]. The addition of 5 wt.% NS increased the LOI by less than 1%. It can be said that applying 5 and 10 bilayers to a PLA surface results in the same effect. In turn, the adsorption of 5 layers onto the composite surface has virtually no effect on LOI values. Although covering both surfaces with 15 bilayers of CS and NS yields a nearly 1.7% increase in LOI, these samples still tend to ignite in oxygen deficiency. This means that by covering the surfaces of PLA and PLA/A200, it was possible to reduce the ignition susceptibility of these biomaterials under reduced oxygen concentration, but the achieved shift of the ignition limit is still too small.

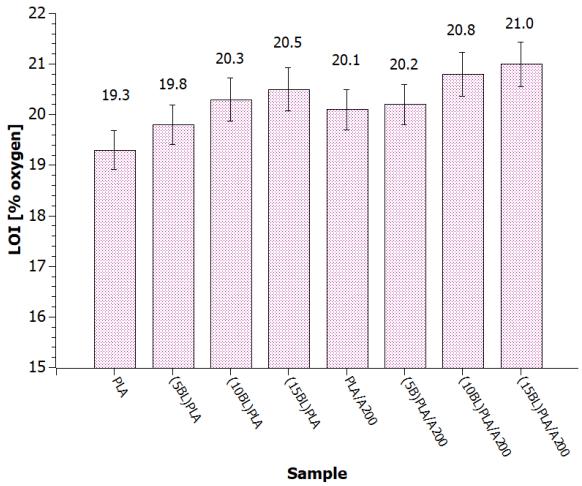

Figure 11. LOI values for all tested biocomposites

7. CONCLUSIONS

The application of the LbL technique for layering chitosan (CS) and nanosilica (NS) has made it possible to achieve a reduction in the flammability of polylactide composites and the biopolymer itself, with a low concentration of adsorbates. The presence of Si-O-Si groups in the vicinity of NH-CO promotes the formation of solid char at temperatures above 350°C. This suggests that by combining natural compounds containing these groups, char-forming flame retardant can be produced. As the applied bilayers, and thus the concentration of Si-O-Si and NH-CO groups on the surface of the biomaterials, increased, the amount of carbonization formed increased. Thus, the mechanism of combustion of the biopolymer visibly changed, where, in addition to the gas and condensed phase, the solid residue appeared. The increased ability to coke at temperatures above 350°C resulted in a heat released rate that was more than 20% lower than that of PLA.

Thus, the charred layer becomes an insulator that divides the internal structures of the material before energy and mass exchange. One of the most important characteristics of a material that controls its fire properties is the amount of gas phase and condensed phase released. Reducing the amount of gas phase released is one of the most effective approaches to blocking combustion. Increasing carbonization reduces the amount of gas and condensed phase released and increases the amount of residue. The consequence of lowering the PHRR was an increase in combustion time, also confirmed by UL-94 testing. In addition, the adsorbed CS-NS bilayers protected the core of the sample from direct flame exposure by shifting the LOI limit by nearly 2% upward.

In conclusion, promising results have been obtained, opening new paths toward the use of bio-flame retardant hybrids dedicated to polylactide and other biopolymers, as well as drawing attention back to the potential of layers deposition using a.o. the LbL technique. In the long term, using the knowledge gained so far, we should focus on designing hybrid multilayer systems that will achieve flammability at least twice as low as that obtained in this publication. It is also worth mentioning that the PLA/A200 composites obtained can also be pyrolyzed at high temperatures, again obtaining a pyrolyzed filler. The circle of life of the filler is then closed. Unfortunately, the yield of NS obtained by pyrolysis is dictated mainly by the concentration of the additive in the input composite.

REFERENCES

[1] Mustapa, I.R., Shanks, R.A., Kong, I., Daud, N. (2018). Morphological structure and thermomechanical properties of hemp fibre reinforced poly (lactic acid) nanocomposites plasticized with tributyl citrate. Materials Today: Proceedings, 5(1): 3211-3218. https://doi.org/10.1016/J.MATPR.2018.01.130

[2] Yang, X.M., Qiu, S., Yusuf, A., Sun, J., Zhai, Z., Zhao, J., Yin, G.Z. (2023). Recent advances in flame retardant and mechanical properties of polylactic acid: A review. International Journal of Biological Macromolecules, 243: 125050. https://doi.org/10.1016/J.IJBIOMAC.2023.125050

[3] Wang, X., Wang, D.Y. (2017). Fire-retardant polylactic acid-based materials: Preparation, properties, and mechanism. Novel Fire Retardant Polymers and Composite Materials, 93-116. https://doi.org/10.1016/B978-0-08-100136-3.00004-2

[4] Ahmed, L., Zhang, B., Hatanaka, L.C., Mannan, M.S. (2018). Application of polymer nanocomposites in the flame retardancy study. Journal of Loss Prevention in the Process Industries, 55: 381-391. https://doi.org/10.1016/J.JLP.2018.07.005

[5] Costes, L., Laoutid, F., Brohez, S., Dubois, P. (2017). Bio-based flame retardants: When nature meets fire protection. Materials Science and Engineering: R: Reports, 117: 1-25. https://doi.org/10.1016/J.MSER.2017.04.001

[6] Costes, L., Laoutid, F., Brohez, S., Delvosalle, C., Dubois, P. (2017). Phytic acid–lignin combination: A simple and efficient route for enhancing thermal and flame retardant properties of polylactide. European Polymer Journal, 94: 270-285. https://doi.org/10.1016/J.EURPOLYMJ.2017.07.018

[7] Cheng, X.W., Guan, J.P., Tang, R.C., Liu, K.Q. (2016). Phytic acid as a bio-based phosphorus flame retardant for poly (lactic acid) nonwoven fabric. Journal of Cleaner Production, 124: 114-119. https://doi.org/10.1016/J.JCLEPRO.2016.02.113

[8] Chen, C., Gu, X., Jin, X., Sun, J., Zhang, S. (2017). The effect of chitosan on the flammability and thermal stability of polylactic acid/ammonium polyphosphate biocomposites. Carbohydrate Polymers, 157: 1586-1593. https://doi.org/10.1016/J.CARBPOL.2016.11.035

[9] Stoleru, E., Hitruc, E.G., Vasile, C., Oprică, L. (2017). Biodegradation of poly (lactic acid)/chitosan stratified composites in presence of the Phanerochaete chrysosporium fungus. Polymer Degradation and Stability, 143: 118-129. https://doi.org/10.1016/J.POLYMDEGRADSTAB.2017.06.023

[10] Kozen, B.G., Kircher, S.J., Henao, J., Godinez, F.S., Johnson, A.S. (2008). An alternative hemostatic dressing: Comparison of CELOX, HemCon, and QuikClot. Academic Emergency Medicine, 15(1): 74-81. https://doi.org/10.1111/J.1553-2712.2007.00009.X

[11] Millner, R.W.J., Lockhart, A.S., Bird, H., Alexiou, C. (2009). A new hemostatic agent: initial life-saving experience with Celox (chitosan) in cardiothoracic surgery. Annals of Thoracic Surgery, 87(2): e13-e14. https://doi.org/10.1016/j.athoracsur.2008.09.046

[12] Raafat, D., Sahl, H.G. (2009). Chitosan and its antimicrobial potential—A critical literature survey. Microbial Biotechnology, 2(2): 186-201. https://doi.org/10.1111/J.1751-7915.2008.00080.X

[13] Yu, M., Chu, Y., Xie, W., Fang, L., Zhang, O., Ren, M., Sun, J. (2024). Phosphorus-containing reactive compounds to prepare fire-resistant vinyl resin for composites: Effects of flame retardant structures on properties and mechanisms. Chemical Engineering Journal, 480: 148167. https://doi.org/10.1016/J.CEJ.2023.148167

[14] Lee, S.H., Oh, S.W., Lee, Y.H., Kim, I.J., Lee, D.J., Lim, J.C., Park, C.C., Kim, H.D. (2020). Preparation and properties of flame-retardant epoxy resins containing reactive phosphorus flame retardant. Journal of Engineered Fibers and Fabrics, 15. https://doi.org/10.1177/1558925020901323

[15] Gaan, S., Sun, G., Hutches, K., Engelhard, M.H. (2008). Effect of nitrogen additives on flame retardant action of tributyl phosphate: Phosphorus–nitrogen synergism. Polymer Degradation and Stability, 93(1): 99-108. https://doi.org/10.1016/J.POLYMDEGRADSTAB.2007.10.013

[16] Wang, D., Liu, Q., Peng, X., Liu, C., Li, Z., Li, Z., Wang, R., Zheng, P., Zhang, H. (2021). High-efficiency phosphorus/nitrogen-containing flame retardant on epoxy resin. Polymer Degradation and Stability, 187: 109544. https://doi.org/10.1016/J.POLYMDEGRADSTAB.2021.109544

[17] Jiang, J., Li, J., Hu, J., Fan, D. (2010). Effect of nitrogen phosphorus flame retardants on thermal degradation of wood. Construction and Building Materials, 24(12): 2633-2637. https://doi.org/10.1016/J.CONBUILDMAT.2010.04.064

[18] Kim, H.H., Sim, M.J., Lee, J.C., Cha, S.H. (2023). The

effects of chemical structure for phosphorus-nitrogen flame retardants on flame retardant mechanisms. Journal of Materials Science, 58: 6850-6864. https://doi.org/10.1007/s10853-023-08414-6
[19] Okamoto, Y., Kawakami, K., Miyatake, K., Morimoto, M., Shigemasa, Y., Minami, S. (2002). Analgesic effects of chitin and chitosan. Carbohydrate Polymers, 49(3): 249-252. https://doi.org/10.1016/S0144-8617(01)00316-2
[20] Goy, R.C., De Britto, D., Assis, O.B.G. (2009). A review of the antimicrobial activity of chitosan. Polímeros, 19(3): 241-247. https://doi.org/10.1590/S0104-14282009000300013
[21] Jiang, W.Z., Cai, Y., Li, H.Y. (2017). Chitosan-based spray-dried mucoadhesive microspheres for sustained oromucosal drug delivery. Powder Technology, 312: 124-132. https://doi.org/10.1016/J.POWTEC.2017.02.021
[22] Li, P., Liu, C., Xu, Y.J., Jiang, Z.M., Liu, Y., Zhu, P. (2020). Novel and eco-friendly flame-retardant cotton fabrics with lignosulfonate and chitosan through LbL: Flame retardancy, smoke suppression and flame-retardant mechanism. Polymer Degradation and Stability, 181: 109302. https://doi.org/10.1016/J.POLYMDEGRADSTAB.2020.109302
[23] Wang, T.C., Jia, M.H., Xu, N.T., Hu, W., Jiang, Z., Zhao, B., Ni, Y.P., Shao, Z.B. (2024). Facile fabrication of adenosine triphosphate/chitosan/polyethyleneimine coating for high flame-retardant lyocell fabrics with outstanding antibacteria. International Journal of Biological Macromolecules, 260: 129599. https://doi.org/10.1016/J.IJBIOMAC.2024.129599
[24] Niu, H., Xiao, Z., Zhang, P., Guo, W., Hu, Y., Wang, X. (2024). Flame retardant, heat insulating and hydrophobic chitosan-derived aerogels for the clean-up of hazardous chemicals. Science of The Total Environment, 908: 168261. https://doi.org/10.1016/J.SCITOTENV.2023.168261
[25] Kumar Kundu, C., Wang, W., Zhou, S., Wang, X., Sheng, H., Pan, Y., Song, L., Hu, Y. (2017). A green approach to constructing multilayered nanocoating for flame retardant treatment of polyamide 66 fabric from chitosan and sodium alginate. Carbohydrate Polymers, 166: 131-138. https://doi.org/10.1016/J.CARBPOL.2017.02.084
[26] Zhang, X., Chen, H., Zhang, H. (2007). Layer-by-layer assembly: From conventional to unconventional methods. Chemical Communications, 14: 1395-1405. https://doi.org/10.1039/B615590A
[27] De Villiers, M.M., Otto, D.P., Strydom, S.J., Lvov, Y.M. (2011). Introduction to nanocoatings produced by layer-by-layer (LbL) self-assembly. Advanced Drug Delivery Reviews, 63(9): 701-715. https://doi.org/10.1016/J.ADDR.2011.05.011
[28] Majka, T.M., Witek, M., Radzik, P., Komisarz, K., Mitoraj, A., Pielichowski, K. (2020). Layer-by-Layer deposition of copper and phosphorus compounds to develop flame-retardant polyamide 6/montmorillonite hybrid composites. Applied Sciences, 10(14): 5007. https://doi.org/10.3390/APP10145007
[29] Ghavidel Mehr, N., Hoemann, C.D., Favis, B.D. (2015). Chitosan surface modification of fully interconnected 3D porous poly (ε-caprolactone) by the LbL approach. Polymer, 64: 112-121. https://doi.org/10.1016/J.POLYMER.2015.03.025
[30] Liu, Y., Wang, Q.Q., Jiang, Z.M., Zhang, C.J., Li, Z.F., Chen, H.Q., Zhu, P. (2018). Effect of chitosan on the fire retardancy and thermal degradation properties of coated cotton fabrics with sodium phytate and APTES by LBL assembly. Journal of Analytical and Applied Pyrolysis, 135: 289-298. https://doi.org/10.1016/J.JAAP.2018.08.024
[31] Ma, X., Wu, N., Liu, P., Cui, H. (2022). Fabrication of highly efficient phenylphosphorylated chitosan bio-based flame retardants for flammable PLA biomaterial. Carbohydrate Polymers, 287: 119317. https://doi.org/10.1016/J.CARBPOL.2022.119317
[32] Vahabi, H., Shabanian, M., Aryanasab, F., Mangin, R., Laoutid, F., Saeb, M.R. (2018). Inclusion of modified lignocellulose and nano-hydroxyapatite in development of new bio-based adjuvant flame retardant for poly(lactic acid). Thermochimica Acta, 666: 51-59. https://doi.org/10.1016/J.TCA.2018.06.004
[33] Jing, J., Zhang, Y., Fang, Z. (2017). Diphenolic acid based biphosphate on the properties of polylactic acid: Synthesis, fire behavior and flame retardant mechanism. Polymer, 108: 29-37. https://doi.org/10.1016/J.POLYMER.2016.11.036
[34] Mahmoud, M.E., Moneim El-Ghanam, A., Saad, S.R. (2023). Fast and efficient adsorptive capture of Congo red and Erythromycin pollutants by a novel nanobiosorbent from crosslinked nanosilica with nanobiochar and chitosan. Inorganic Chemistry Communications, 158: 111557. https://doi.org/10.1016/J.INOCHE.2023.111557
[35] Liu, Y., Cai, Z., Sheng, L., Ma, M., Xu, Q. (2019). Influence of nanosilica on inner structure and performance of chitosan based films. Carbohydrate Polymers, 212: 421-429. https://doi.org/10.1016/J.CARBPOL.2019.02.079
[36] Wu, R., Abdulhameed, A.S., Jawad, A.H., Yong, S.K., Li, H., ALOthman, Z.A., Wilson, L.D., Algburi, S. (2023). Development of a chitosan/nanosilica biocomposite with arene functionalization via hydrothermal synthesis for acid red 88 dye removal. International Journal of Biological Macromolecules, 252: 126342. https://doi.org/10.1016/J.IJBIOMAC.2023.126342
[37] Yan, K., Liu, C., Ma, J. (2021). Dendritic fibrous nanosilica loaded chitosan for improving water vapor permeability and antibacterial properties of waterborne polyurethane acrylate membranes. Journal of Cleaner Production, 291: 125922. https://doi.org/10.1016/J.JCLEPRO.2021.125922
[38] Liu, Y., Cai, Z., Sheng, L., Ma, M., Xu, Q. (2019). Influence of nanosilica on inner structure and performance of chitosan based films. Carbohydrate Polymers, 212: 421-429. https://doi.org/10.1016/J.CARBPOL.2019.02.079
[39] Podust, T.V., Kulik, T.V., Palyanytsya, B.B., Gun'Ko, V.M., Tóth, A., Mikhalovska, L., Menyhárd, A., László, K. (2014). Chitosan-nanosilica hybrid materials: Preparation and properties. Applied Surface Science, 320: 563-569. https://doi.org/10.1016/J.APSUSC.2014.09.038
[40] Ismail, M.Y., Patanen, M., Sirviö, J.A., Visanko, M., Ohigashi, T., Kosugi, N., Huttula, M., Liimatainen, H. (2019). Hybrid films of cellulose nanofibrils, chitosan

and nanosilica—Structural, thermal, optical, and mechanical properties. Carbohydrate Polymers, 218: 87-94. https://doi.org/10.1016/J.CARBPOL.2019.04.065
[41] da Luz, R.C.S., Paixão, M.V.G., de C. Balaban, R. (2019). Nanosilica-chitosan hybrid materials: Preparation, characterization and application in aqueous drilling fluids. Journal of Molecular Liquids, 279: 279-288. https://doi.org/10.1016/J.MOLLIQ.2019.01.131
[42] Hao, X., Kaschta, J., Pan, Y., Liu, X., Schubert, D.W. (2016). Intermolecular cooperativity and entanglement network in a miscible PLA/PMMA blend in the presence of nanosilica. Polymer, 82: 57-65. https://doi.org/10.1016/J.POLYMER.2015.11.029
[43] Ortenzi, M.A., Basilissi, L., Farina, H., Di Silvestro, G., Piergiovanni, L., Mascheroni, E. (2015). Evaluation of crystallinity and gas barrier properties of films obtained from PLA nanocomposites synthesized via "in situ" polymerization of l-lactide with silane-modified nanosilica and montmorillonite. European Polymer Journal, 66: 478-491. https://doi.org/10.1016/J.EURPOLYMJ.2015.03.006
[44] Majka, T.M., Pimentel, A.C., Fernandes, S., de Almeida, H.V., Borges, J.P., Martins, R. (2024). Experimental consideration of the effects of calcium lignosulfonate and tannic acid on the flammability and thermal properties of polylactide composites. Thermochimica Acta, 737: 179769. https://doi.org/10.1016/J.TCA.2024.179769
[45] Lee, D.W., Lim, C., Israelachvili, J.N., Hwang, D.S. (2013). Strong adhesion and cohesion of chitosan in aqueous solutions. Langmuir, 29(46): 14222-14229. https://doi.org/10.1021/la403124u
[46] Kan, Y., Yang, Q., Tan, Q., Wei, Z., Chen, Y. (2020). Diminishing cohesion of chitosan films in acidic solution by multivalent metal cations. Langmuir, 36(18): 4964-4974. https://doi.org/10.1021/acs.langmuir.0c00438
[47] Roy, P.S., Samanta, A., Mukherjee, M., Roy, B., Mukherjee, A. (2013). Designing novel pH-induced chitosan-gum odina complex coacervates for colon targeting. Industrial and Engineering Chemistry Research, 52(45): 15728-15745. https://doi.org/10.1021/ie401681t
[48] Pham, T.D., Bui, T.T., Nguyen, V.T., Van Bui, T.K., Tran, T.T., Phan, Q.C., Pham, T.D., Hoang, T.H. (2018). Adsorption of polyelectrolyte onto nanosilica synthesized from rice husk: Characteristics, mechanisms, and application for antibiotic removal. Polymers, 10(2): 220. https://doi.org/10.3390/POLYM10020220
[49] Gustave, T., Chantale Njiomou, D., Charles Fon, A., Danie Laure Mbella, M., Guillonnel Trésor Nyadjou, D., Jean Marie, K., Philippe, B. (2022). Nano-silica from kaolinitic clay used as adsorbent for anionic and cationic dyes removal: Linear and non-linear regression isotherms and kinetics studies. Annals of Civil and Environmental Engineering, 6: 008-018. https://doi.org/10.29328/JOURNAL.ACEE.1001034
[50] Malewska, E., Prociak, A. (2015). The effect of nanosilica filler on the foaming process and properties of flexible polyurethane foams obtained with rapeseed oil-based polyol. Polimery, 60(7-8): 472-479. https://doi.org/10.14314/POLIMERY.2015.472
[51] Pan, P., Inoue, Y. (2009). Polymorphism and isomorphism in biodegradable polyesters. Progress in Polymer Science, 34(7): 605-640. https://doi.org/10.1016/J.PROGPOLYMSCI.2009.01.003
[52] Sasaki, S., Asakura, T. (2003). Helix distortion and crystal structure of the α-form of poly(l-lactide). Macromolecules, 36(22): 8385-8390. https://doi.org/10.1021/MA0348674
[53] Puiggali, J., Ikada, Y., Tsuji, H., Cartier, L., Okihara, T., Lotz, B. (2000). The frustrated structure of poly(l-lactide). Polymer, 41(25): 8921-8930. https://doi.org/10.1016/S0032-3861(00)00235-4
[54] Kazuyo, D.S., Aki Sasashige, T., Kanamoto, T., Hyon, S.H. (2003). Preparation of oriented β-form poly (l-lactic acid) by solid-state coextrusion: Effect of extrusion variables. Macromolecules, 36(10): 3601-3605. https://doi.org/10.1021/MA030050Z
[55] Cartier, L., Okihara, T., Ikada, Y., Tsuji, H., Puiggali, J., Lotz, B. (2000). Epitaxial crystallization and crystalline polymorphism of polylactides. Polymer, 41(25): 8909-8919. https://doi.org/10.1016/S0032-3861(00)00234-2
[56] Zhang, J., Duan, Y., Sato, H., Tsuji, H., Noda, I., Yan, S., Ozaki, Y. (2005). Crystal modifications and thermal behavior of poly (l-lactic acid) revealed by infrared spectroscopy. Macromolecules, 38(19): 8012-8021. https://doi.org/10.1021/MA051232R
[57] Cho, T.Y., Strobl, G. (2006). Temperature dependent variations in the lamellar structure of poly(l-lactide). Polymer, 47(4): 1036-1043. https://doi.org/10.1016/J.POLYMER.2005.12.027
[58] Zhang, J., Tsuji, H., Noda, I., Ozaki, Y. (2004). Structural changes and crystallization dynamics of poly (l-lactide) during the cold-crystallization process investigated by infrared and two-dimensional infrared correlation spectroscopy. Macromolecules, 37(17): 6433-6439. https://doi.org/10.1021/MA049288T
[59] Zhang, J., Tsuji, H., Noda, I., Ozaki, Y. (2004). Weak intermolecular interactions during the melt crystallization of poly (l-lactide) investigated by two-dimensional infrared correlation spectroscopy. Journal of Physical Chemistry B, 108(31): 11514-11520. https://doi.org/10.1021/JP048308Q
[60] Liu, X., Gu, X., Sun, J., Zhang, S. (2017). Preparation and characterization of chitosan derivatives and their application as flame retardants in thermoplastic polyurethane. Carbohydrate Polymers, 167: 356-363. https://doi.org/10.1016/J.CARBPOL.2017.03.011
[61] Majka, T.M., Piech, R., Piechaczek, M., Ostrowski, K.A. (2024). The influence of Urtica dioica and Vitis vinifera fibers on the thermal properties and flammability of polylactide composites. Materials, 17(6): 1256. https://doi.org/10.3390/MA17061256
[62] Majka, T.M. (2023). The influence of amino chain length and calcium lignosulfonate modification on lignosulfonamides flammability and thermal stability. Polimery, 68(10): 544-554. https://doi.org/10.14314/POLIMERY.2023.10.4
[63] Majka, T.M. (2023). Flammability analysis of poly (ethylene terephthalate) and recycled PET with pyrolyzed filler. Journal of Polymer Research, 30: 1-19. https://doi.org/10.1007/S10965-023-03737-Z/TABLES/7
[64] Chen, J., Liu, Z., Qiu, S., Li, Y., Sun, J., Li, H., Gu, X., Zhang, S. (2023). A new strategy for the preparation of polylactic acid composites with flame retardancy, UV resistance, degradation, and recycling performance. Chemical Engineering Journal, 472: 145000.

https://doi.org/10.1016/J.CEJ.2023.145000
[65] Rahatekar, S.S., Zammarano, M., Matko, S., Koziol, K.K., Windle, A.H., Nyden, M., Kashiwagi, T., Gilman, J.W. (2010). Effect of carbon nanotubes and montmorillonite on the flammability of epoxy nanocomposites. Polymer Degradation and Stability, 95(5): 870-879. https://doi.org/10.1016/J.POLYMDEGRADSTAB.2010.01.003